Supporting information

Role of surface hydroxyl species in copper catalyzed hydrogenation of ketones

Jenoff E. De Vrieze, Joris Thybaut, Mark Saeys*

Laboratory for Chemical Technology, Ghent University, Technologiepark 914, 9052 Gent, Belgium

Corresponding Author

*Email address: mark.saeys@ugent.be

Telephone no: +32 (0)9 331 17 54

Table of Contents

1. Benchmark calculations

To select an appropriate functional, benchmark calculations were performed for the adsorption of CH_3O, a model alkoxy species, and of CH_3OH on Pt(111), and for the adsorption of CO on Cu(111). The binding energy for CH_3O and CH_3OH on Pt(111) was compared with Single Crystal Adsorption Calorimetry (SCAC) data from Campbell et al.[1], while the CO adsorption energy on Cu(111) was compared with thermal desorption spectroscopy data[2-3].The calculations show that the VdW-DF2 functional provides an accurate description for the adsorption of alcohols and alkoxy species on Pt(111), and for CO on Cu(111). The PBE functional underestimates the strength of alcohol and alkoxy adsorption, but overestimates the strength of CO adsorption.

Table S1. Comparison of VdW-DF2 and PBE binding energies for CH_3O and CH_3OH on Pt(111) with Single Crystal Adsorption Calorimetry data.

	VdW-DF2 [kJmol^{-1}]	PBE [kJmol^{-1}]	Exp[1] [kJmol^{-1}]
CH_3O	-176	-166	-187 +/- 11
CH_3OH	-52	-34	-60

Table S2. Adsorption energy and site preference for CO on Cu(111).

	Site preference	E_{ads} [kJmol^{-1}]
PBE	top	-68
BEEF-VdW	hollow fcc	-49
VdW-DF2	top	-42
Exp[2-3]	top	-44 and -47

2. Sensitivity of the low-coverage microkinetic model to the stability of different species
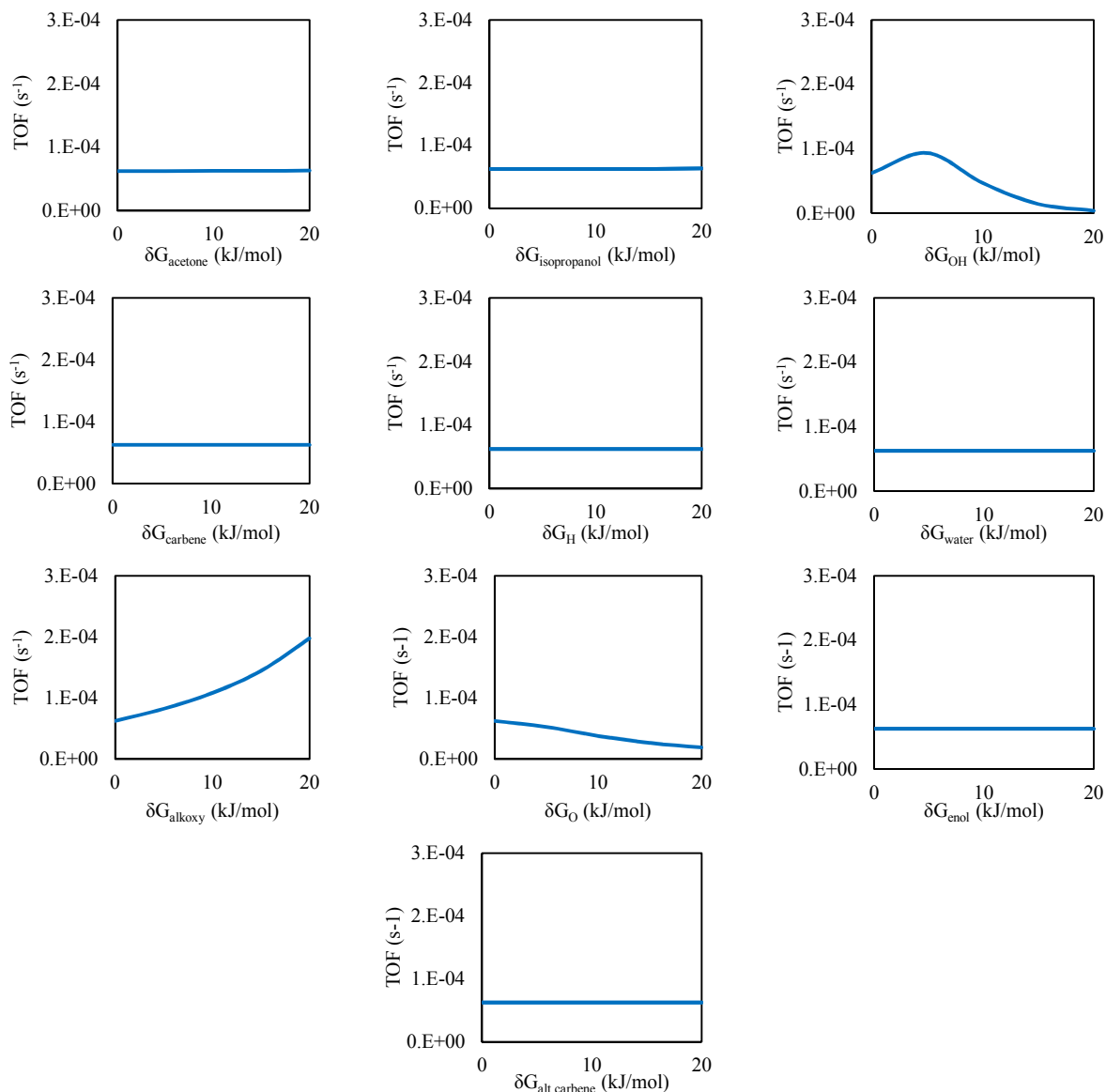

Figure S1. Effect of the stability of the various intermediates on the calculated turnover-frequency for the low-coverage microkinetic model (Table 2 and 3).

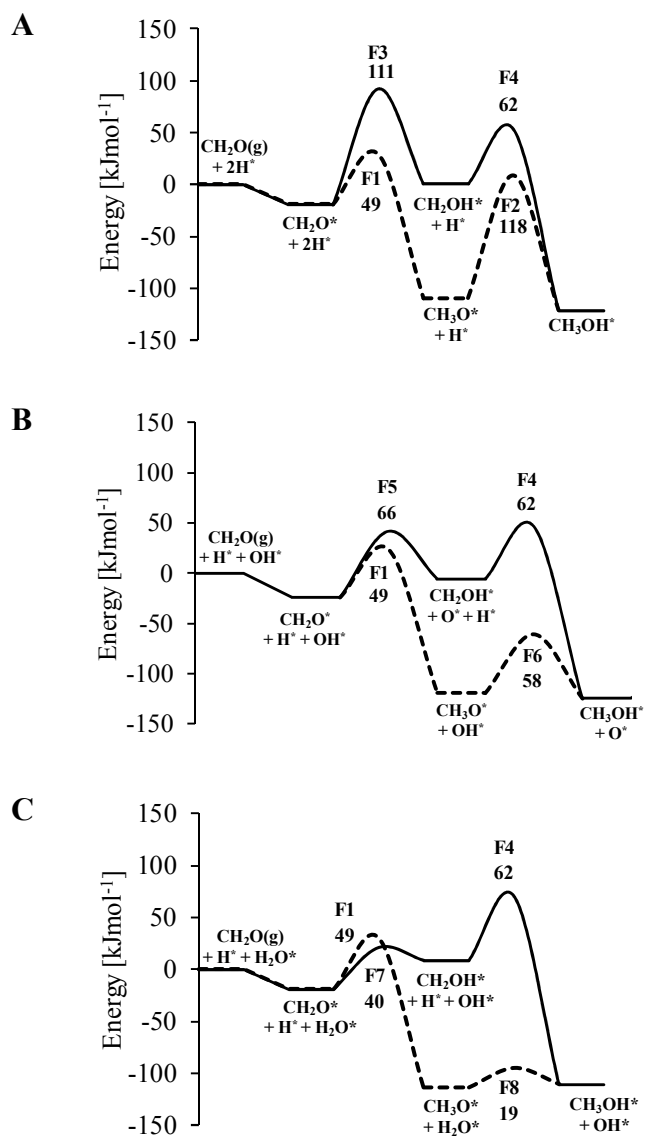## 3. Energy diagram for formaldehyde hydrogenation

Figure S2. Energy profiles for the hydrogenation of formaldehyde to methanol on Cu(111) with surface hydrogen (A), with surface hydroxyl (B) and with surface water (C). The dashed line corresponds to the alkoxy pathway, the full line to the carbene pathway. The corresponding transition state structures are shown in Figure S3.
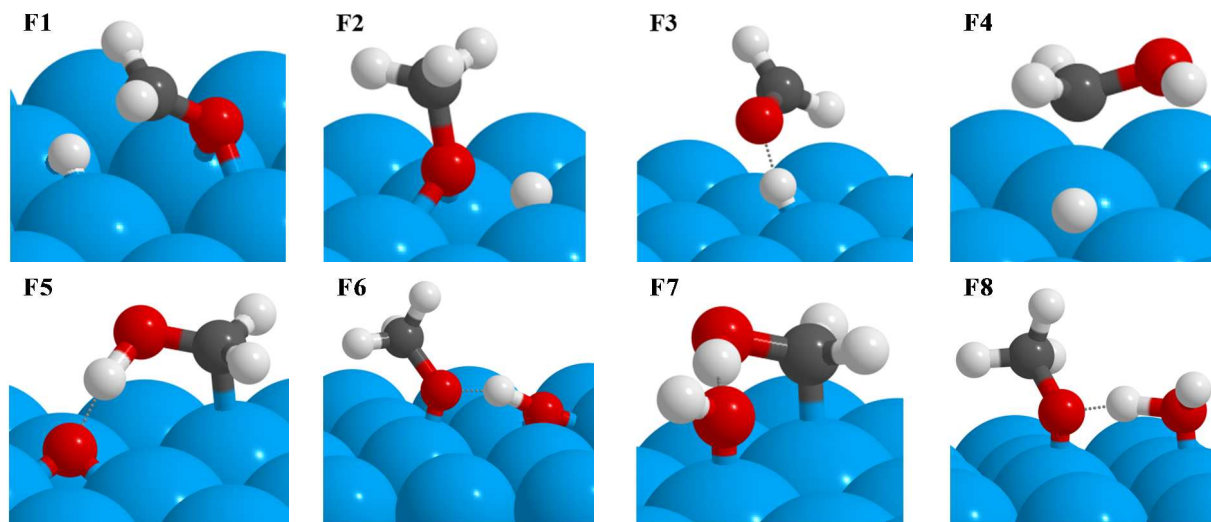
Figure S3. Transition states for the various possible formaldehyde hydrogenation pathways on Cu(111). Top row: Hydrogenation of the carbonyl C and O atom by atomic hydrogen; second row: hydrogenation of the carbonyl O atom by a surface hydroxyl and by water.
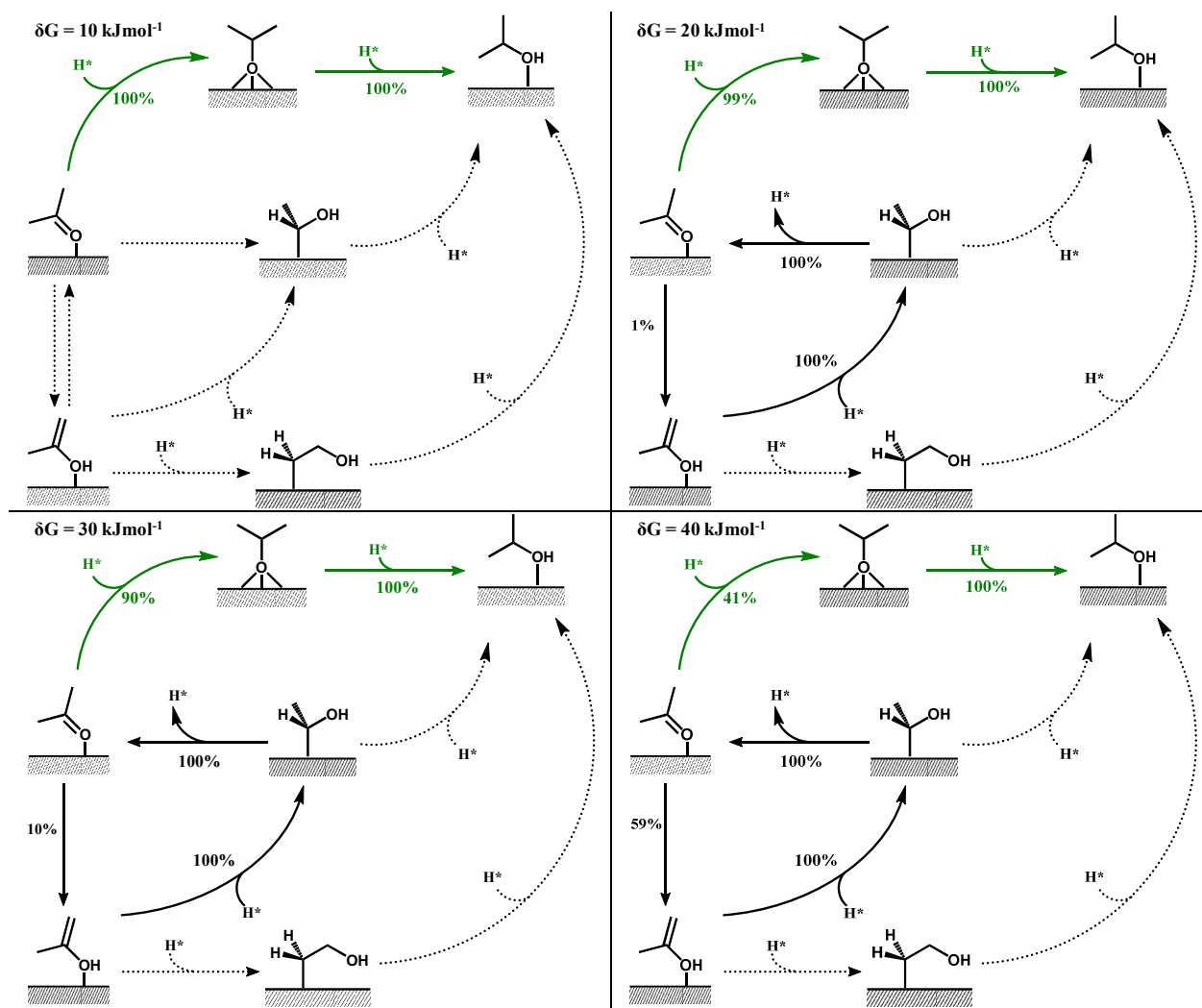
4. Role of the enol hydrogenation pathway

Figure S4. Effect of the stability of the enol intermediate on the reaction path analysis for the hydrogenation of acetone to isopropanol in the absence of water. The numbers indicate the fraction of each component consumed in the particular reaction step. Dotted arrows indicate reaction steps that are insignificant, i.e., a fraction below 0.5%, while green arrows indicate reaction steps with a fraction above 90%. Conditions: 500 kg_{cat} s $mol_{acetone}^{-1}$, 473 K, 100 bar, inlet molar ratio: H_2:acetone = 2.

5. Sensitivity of the coverage-dependent microkinetic model to the transfer coefficient in the Brønsted-Evans-Polanyi relation

The destabilization of the reaction intermediates in the coverage-dependent microkinetic model affects the reaction free energies for the various steps. We used the Brønsted-Evans-Polanyi relationship.[4]

$$E_a = E_0 + \alpha \Delta H_r$$

to translate the change in stability of the intermediates into a change in the activation energy. We used a transfer coefficient α of 0.5, typical for reactions where the transition state is neither early nor late. The sensitivity of the calculated TOF to the value of the transfer coefficient is shown in Table S3. The reaction path analysis did not change significantly for transfer coefficients between 0.40 and 0.60.

Table S3. Effect of the BEP transfer coefficient on the TOF of the coverage-dependent microkinetic model. Conditions: 500 kg_{cat} s $mol_{acetone}^{-1}$, 473 K, 100 bar, inlet molar ratio: H_2:acetone:H_2O=2:1:0.5

α[-]	TOF change compared to $\alpha = 0.5$
0.40	13%
0.45	7%
0.50	0%
0.55	-8%
0.60	-15%

6. Structures used to determine the coverage-dependent stabilities.

| 1/16 ML | 1/9 ML | 2/9 ML | 1/4 ML |
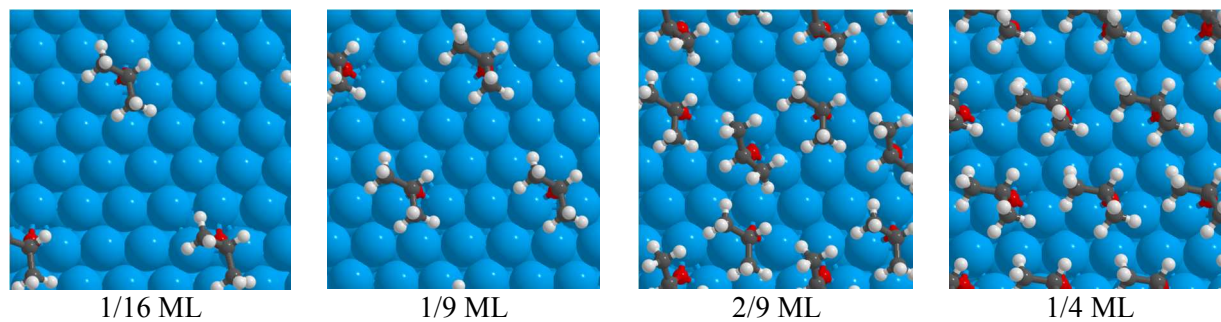
Figure S5. Structures for the alkoxy intra-species repulsion correlation: 1/16, 1/9, 2/9 and 1/4 ML coverage.

| 1/16 ML | 1/9 ML | 2/9 ML | 3/9 ML |

| 4/9 ML | 5/9 ML |

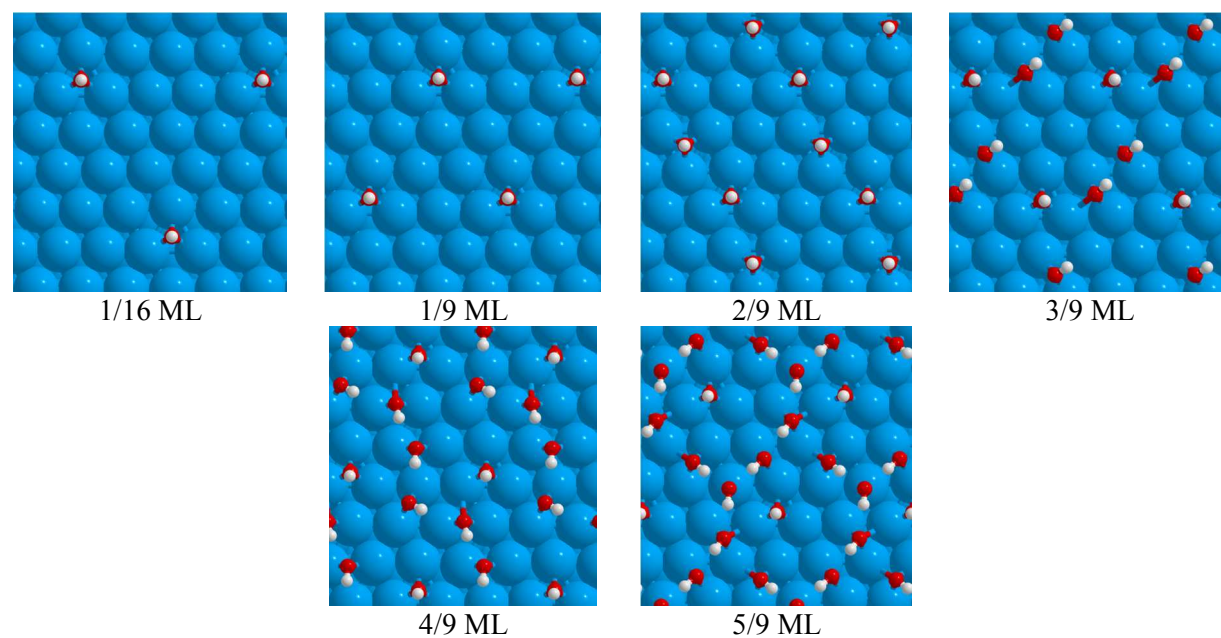**Figure S6**. Structures for the the hydroxyl intra-species repulsion correlation: 1/16, 1/9, 2/9, 3/9, 4/9 and 5/9 ML hydroxyl.
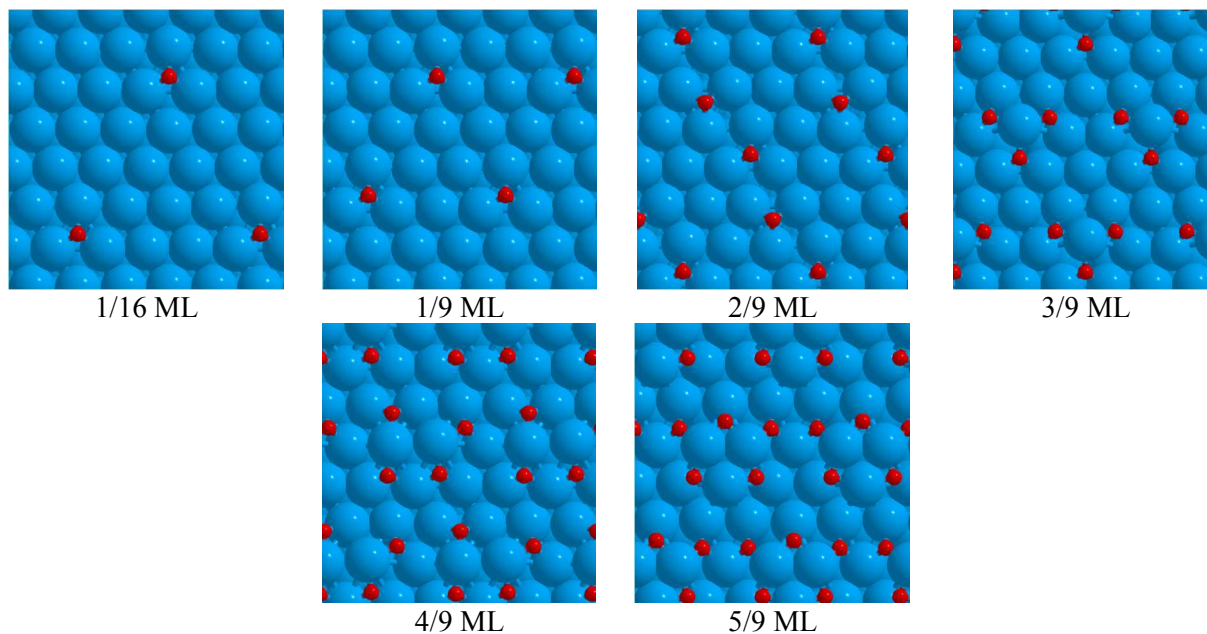
1/16 ML	1/9 ML	2/9 ML	3/9 ML

4/9 ML	5/9 ML

Figure S7. Structures for the oxygen intra-species repulsion correlation: 1/16, 1/9, 2/9, 3/9, 4/9 and 5/9 ML oxygen coverage.
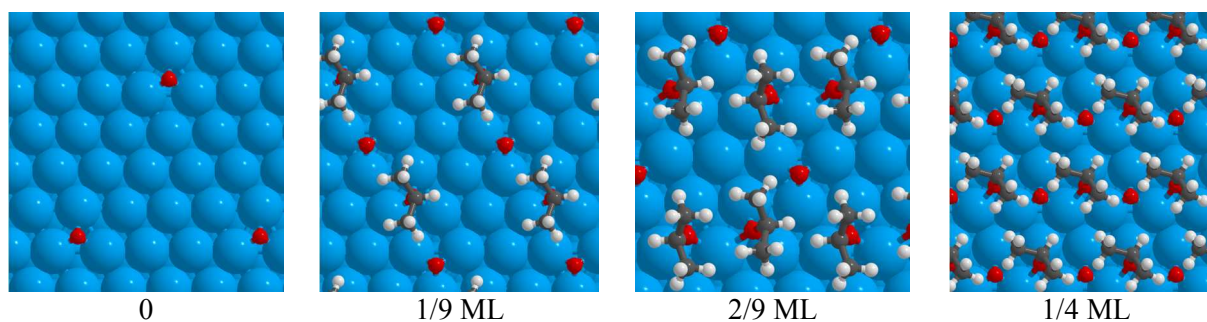

0	1/9 ML	2/9 ML	1/4 ML

Figure S8. Structures for the effect of the alkoxy coverage on the oxygen stability.

<div align="center">0   1/9 ML   2/9 ML</div>

Figure S9. Structures for the effect of the alkoxy coverage on the hydroxyl stability.
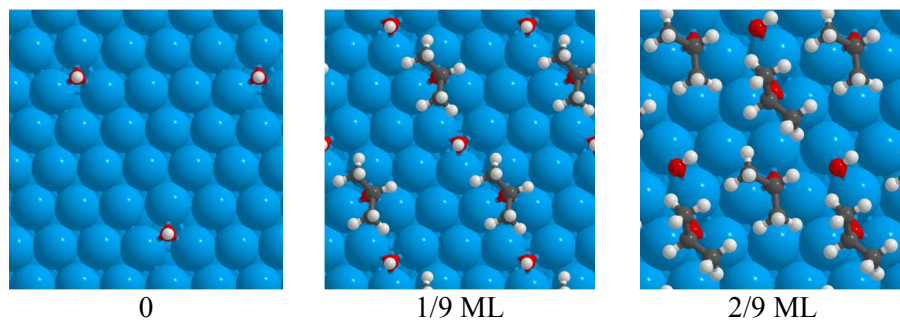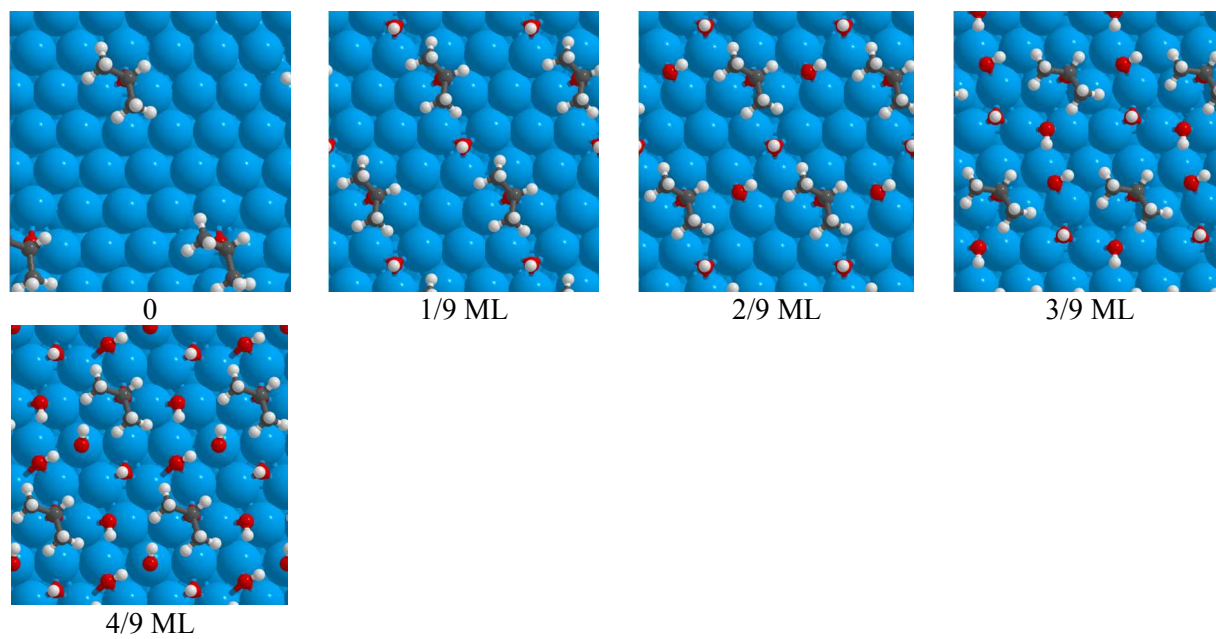

<div align="center">0   1/9 ML   2/9 ML   3/9 ML</div>

<div align="center">4/9 ML</div>

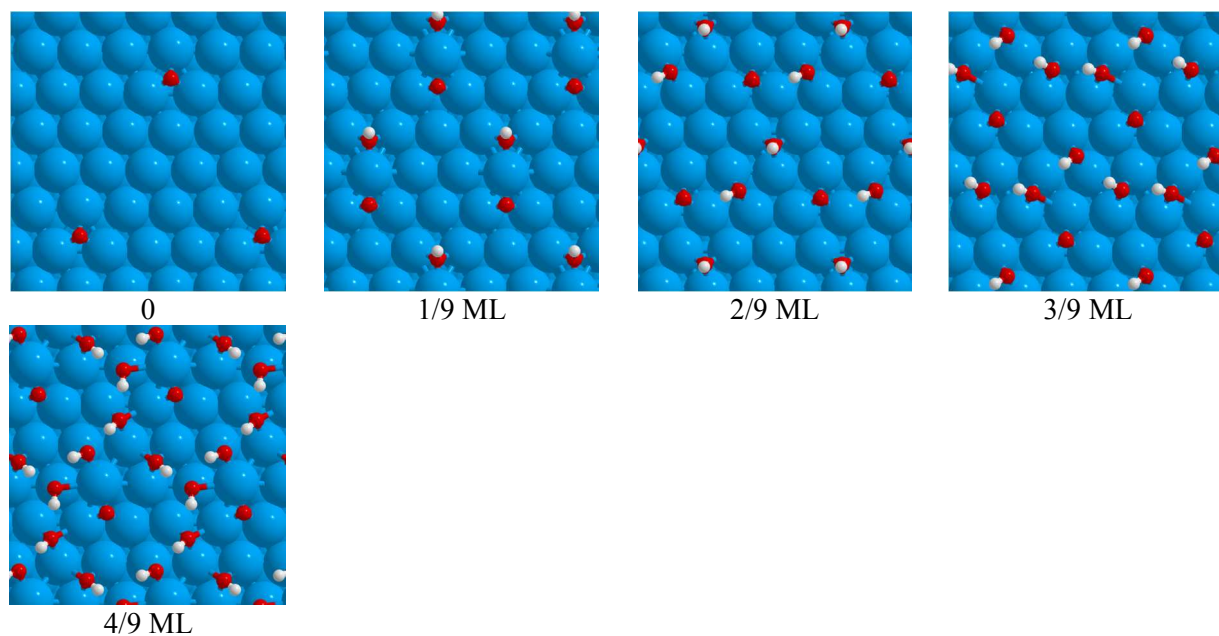**Figure S10**. Structures for the effect of hydroxyl coverage on the alkoxy stability.

0	1/9 ML	2/9 ML	3/9 ML

4/9 ML

Figure S11. Structures for the effect of hydroxyl coverage on the oxygen stability.

0	1/9 ML	2/9 ML	3/9 ML

4/9 ML
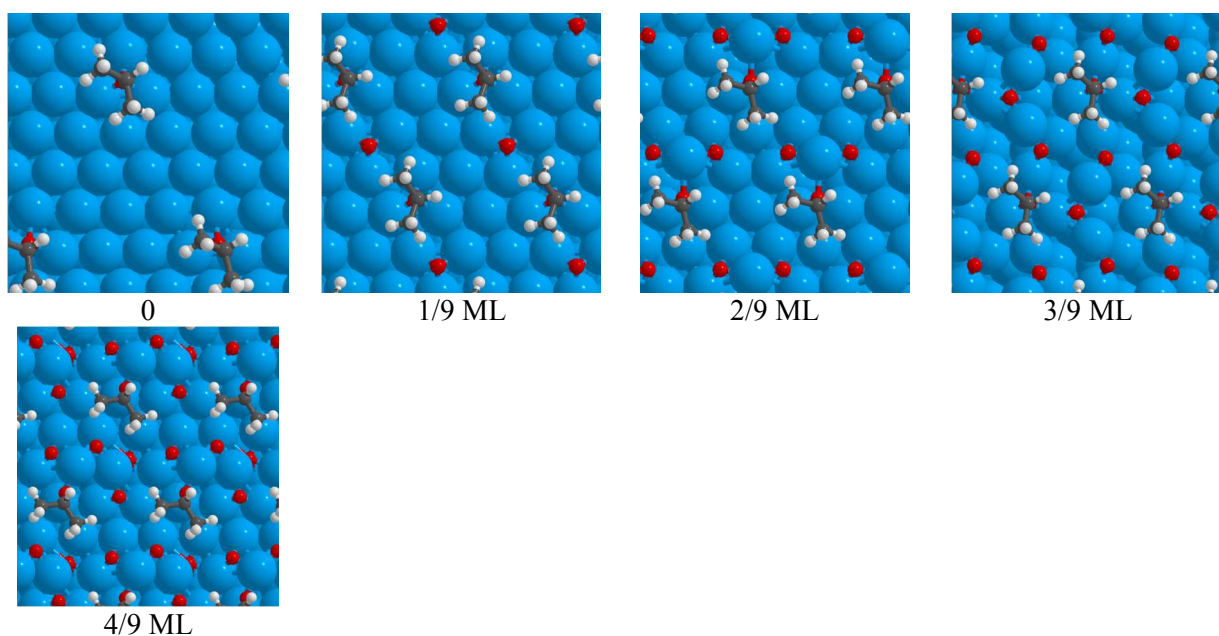
Figure S12. Structures for the effect of oxygen coverage on the alkoxy stability.

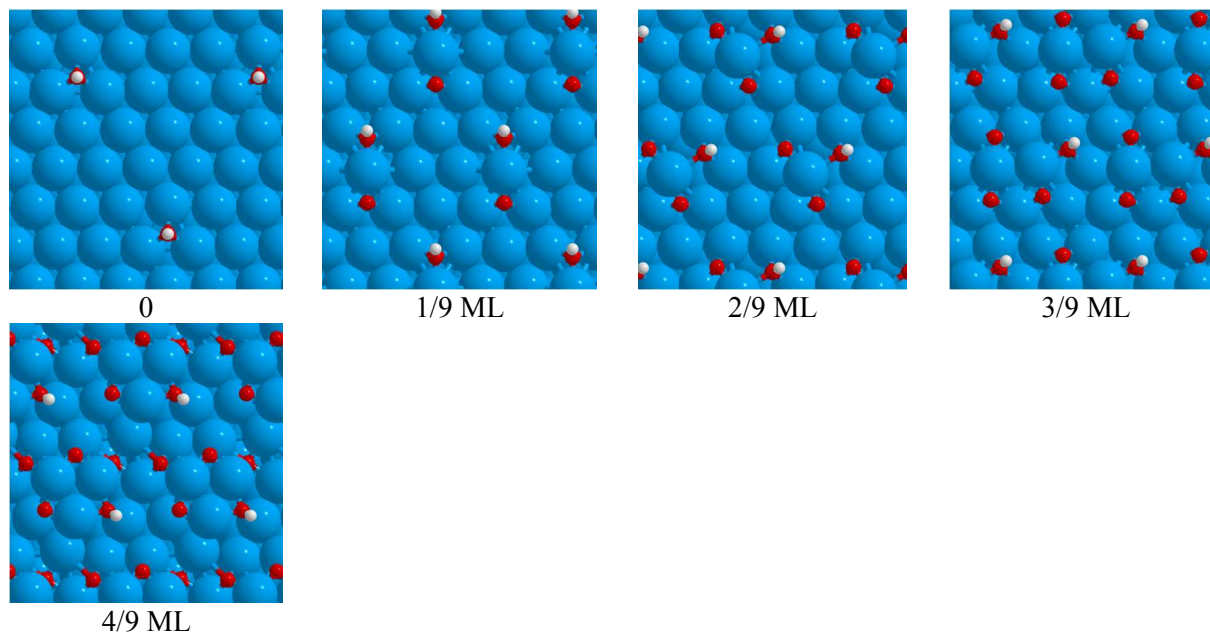0   1/9 ML   2/9 ML   3/9 ML

4/9 ML

Figure S13. Structures for the effect of the oxygen coverage on the hydroxyl stability.

7. Correlations for the repulsion correction relationships

Table S4. Intra-species and inter-species repulsion correction relationships and corresponding R^2 values.

Intra-species repulsion (kJmol^{-1})		R^2 (-)
θ_O on O*	$\delta G_O = 974 \left(\theta_O - \dfrac{1}{16} \right)^{3.5}$	0.99
θ_{OH} on OH*	$\delta G_{OH} = 32 \left(\theta_{OH} - \dfrac{1}{16} \right)^{1.25}$	0.94
θ_{alkoxy} on alkoxy	$\delta G_{alkoxy} = 1228 \left(\theta_{alkoxy} - \dfrac{1}{16} \right)$	0.94
Inter-species repulsion (kJmol^{-1})		**R^2 (-)**
θ_O on OH*	$\delta G_{OH,O} = 374\theta_O^{2.49}$	0.99
θ_{OH} on O*	$\delta G_{O,OH} = 249\theta_{OH}^{2.04}$	0.99
θ_O on alkoxy	$\delta G_{alkoxy,O} = 1199\theta_O^{3.15}$	0.99
θ_{alkoxy} on O*	$\delta G_{O,alkoxy} = 1685\theta_{alkoxy}^{4.34}$	0.99
θ_{OH} on alkoxy	$\delta G_{alkoxy,OH} = 149\theta_{OH}^{1.25}$	0.98
θ_{alkoxy} on OH*	$\delta G_{OH,alkoxy} = 497\theta_{alkoxy}^{1.88}$	0.99

References

1.   Karp, E. M.; Silbaugh, T. L.; Crowe, M. C.; Campbell, C. T., Energetics of Adsorbed Methanol and Methoxy on Pt(111) by Microcalorimetry. *JACS* **2012,** *134*, 20388-20395.

2.   Vollmer, S.; Witte, G.; Wöll, C., Determination of site specific adsorption energies of CO on copper. *Catal. Lett.* **2001,** *77*, 97-101.

3.   Kessler, J.; Thieme, F., Chemisorption of CO on differently prepared Cu (111) surfaces. *Surf. Sci.* **1977,** *67*, 405-415.

4.   Chorkendorff, I.; Niemantsverdriet, J. W., *Concepts of Modern Catalysis and Kinetics*. Wiley: 2003.